Thermodynamic properties of the Shastry-Sutherland model from quantum Monte Carlo simulations

Stefan Wessel,[1] Ido Niesen,[2] Jonas Stapmanns,[1] B. Normand,[3] Frédéric Mila,[4] Philippe Corboz,[2] and Andreas Honecker[5]

[1]*Institut für Theoretische Festkörperphysik, JARA-FIT and JARA-HPC, RWTH Aachen University, 52056 Aachen, Germany*
[2]*Institute for Theoretical Physics and Delta Institute for Theoretical Physics, University of Amsterdam,*
Science Park 904, 1098 XH Amsterdam, The Netherlands
[3]*Neutrons and Muons Research Division, Paul Scherrer Institute, 5232 Villigen-PSI, Switzerland*
[4]*Institute of Theoretical Physics, Ecole Polytechnique Fédérale Lausanne (EPFL), 1015 Lausanne, Switzerland*
[5]*Laboratoire de Physique Théorique et Modélisation, CNRS UMR 8089, Université de Cergy-Pontoise, 95302 Cergy-Pontoise Cedex, France*

We investigate the minus-sign problem that afflicts quantum Monte Carlo (QMC) simulations of frustrated quantum spin systems, focusing on spin $S = 1/2$, two spatial dimensions, and the extended Shastry-Sutherland model. We show that formulating the Hamiltonian in the diagonal dimer basis leads to a sign problem that becomes negligible at low temperatures for small and intermediate values of the ratio of the inter- and intradimer couplings. This is a consequence of the fact that the product state of dimer singlets is the exact ground state both of the extended Shastry-Sutherland model and of a corresponding "sign-problem-free" model, obtained by changing the signs of all positive off-diagonal matrix elements in the dimer basis. By exploiting this insight, we map the sign problem throughout the extended parameter space from the Shastry-Sutherland to the fully frustrated bilayer model and compare it with the phase diagram computed by tensor-network methods. We use QMC to compute with high accuracy the temperature dependence of the magnetic specific heat and susceptibility of the Shastry-Sutherland model for large systems up to a coupling ratio of 0.526(1) and down to zero temperature. For larger coupling ratios, our QMC results assist us in benchmarking the evolution of the thermodynamic properties by systematic comparison with exact diagonalization calculations and interpolated high-temperature series expansions.

I. INTRODUCTION

Frustrated quantum magnets, meaning those in which local exchange processes are in competition, are known to host a rich variety of physical phenomena within unconventional ground states ranging from various kinds of valence-bond crystal to quantum spin liquids [1–4]. However, the investigation of frustrated quantum spin models constitutes a real challenge, because there exist, in general, no unbiased methods by which to study their properties on sufficiently large lattices and at appropriately low temperatures. In two dimensions, quantum Monte Carlo (QMC) is the method of choice for studying the thermal properties of unfrustrated systems such as the square-lattice quantum antiferromagnet [5,6]. In frustrated models, QMC suffers from a very severe "minus-sign" problem when performed in the standard basis of spin configurations, making it essentially impossible to obtain accurate results for any temperatures significantly below the typical coupling constants, which unfortunately constitute the only regime of interest in the context of exotic quantum physics.

Two paradigmatic two-dimensional (2D) spin-1/2 frustrated models with approximate experimental realizations are the kagome antiferromagnet and the Shastry-Sutherland model [7], the first as a candidate quantum spin liquid [8] and the second because of the remarkable, and still hotly debated, series of magnetization plateaus observed in $SrCu_2(BO_3)_2$ [9–17]. Both models have triangles as their building blocks, and

hence a severe QMC sign problem. There is, however, also an important difference between them. While the ground state of the spin-1/2 kagome antiferromagnet is still highly controversial, the ground state of the Shastry-Sutherland model has been known for nearly 40 years [7,18,19]. This model was actually constructed by Shastry and Sutherland as a 2D generalization of the spin-1/2 Majumdar-Ghosh chain [20–22], i.e., explicitly to have a product state of dimer singlets as the ground state. It seems logical to expect that knowledge of the ground state should help very significantly in investigating the low-temperature thermodynamics, but to date this has not been the case. Interpretation of the temperature dependence of the magnetic susceptibility [9] and specific heat of $SrCu_2(BO_3)_2$ [23], the nearly exact realization of the Shastry-Sutherland model, still relies primarily on exact diagonalization (ED) results [19,24,25] obtained for small lattices of up to only 20 sites.[1]

In this paper, we show that knowing the exact ground state of the Shastry-Sutherland model is indeed a considerable advantage, provided that one formulates QMC simulations in the dimer basis [28–32] rather than the conventional site basis.

---

[1]The magnetic susceptibility, $\chi(T)$, has also been analyzed by series expansions [19,26,27], but these are accurate only for temperatures above the maximum of χ.
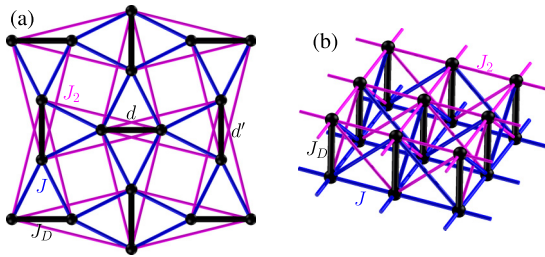
FIG. 1. Schematic representations of the extended Shastry-Sutherland model [Eq. (2)] in (a) single-plane and (b) bilayer format.

Unlike a number of fully frustrated models studied recently, in which the minus sign disappears completely in the dimer basis, we illustrate the extent to which the sign problem is still present throughout the generalized phase diagram that connects the Shastry-Sutherland model to the fully frustrated bilayer. Our key result is that, as long as the product of dimers is not only the ground state of the model itself, but also of the "sign-problem-free" model obtained by changing the sign of the positive off-diagonal matrix elements in the dimer basis, the sign problem decreases at low temperatures and disappears completely at zero temperature. From this insight, we demonstrate using the example of the Shastry-Sutherland model that it is, in fact, possible to perform efficient QMC simulations to study the thermodynamics of certain frustrated quantum systems.

Our paper is organized as follows. In Sec. II, we introduce the Shastry-Sutherland model, the sign-problem-free counterpart model that provides insight into the nature of the minus-sign problem, and the extended model that interpolates between the Shastry-Sutherland case and the fully frustrated bilayer model, which enables us to discuss the ground-state phase diagram. In Sec. III, we exploit the sign-problem-free model to investigate the minus sign in the Shastry-Sutherland model by simulations in the dimer basis, from which we show how the sign problem is suppressed at low temperature in a large portion of the singlet-product phase. In Sec. IV, we build on this observation to compute the low-temperature specific heat and susceptibility of the Shastry-Sutherland model with high accuracy up to the critical coupling ratio. Section V contains a brief summary and perspective. Two appendices provide details of tensor-network and high-temperature series-expansion methods, which we use to augment and benchmark our QMC analysis.

II. THE MODELS

The Shastry-Sutherland model [7], also known as the orthogonal dimer model [25], is defined by the Hamiltonian

$$H = J_D \sum_{\langle i,j \rangle} \vec{S}_i \cdot \vec{S}_j + J \sum_{\langle\langle i,j \rangle\rangle} \vec{S}_i \cdot \vec{S}_j, \qquad (1)$$

where J_D is the intradimer coupling (denoted by $\langle ij \rangle$) and the interdimer coupling ($\langle\langle ij \rangle\rangle$), J, defines a square lattice as shown in Fig. 1(a). For small and intermediate coupling ratios, J/J_D, the ground state is an exact product of singlets formed on the dimer bonds [7].
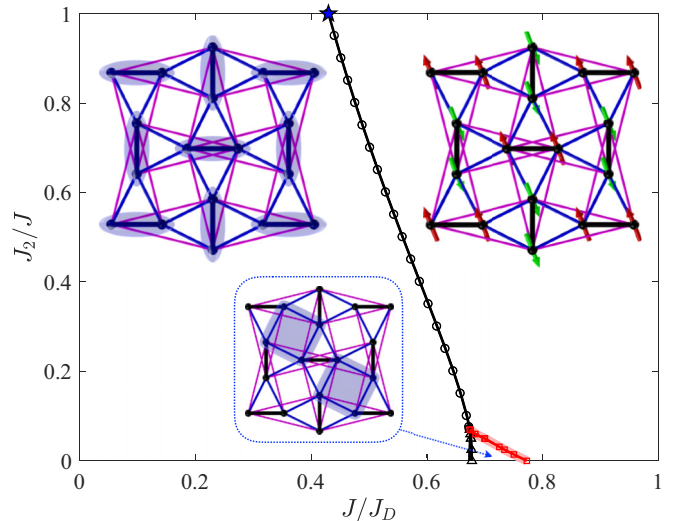

FIG. 2. Ground-state phase diagram of the extended Shastry-Sutherland model of Eq. (2), obtained from iPEPS calculations. All phase transitions are first order. The star at $(J/J_D, J_2/J) = (2.3279(1), 1)$ denotes the location of the quantum phase transition in the fully frustrated bilayer, taken from Ref. [38]. Insets show schematic representations of the dimer singlet-product phase (upper left), the square-lattice antiferromagnetic phase (upper right), and the intermediate plaquette phase (lower).

This is a property that the Shastry-Sutherland model shares with the fully frustrated $S = 1/2$ bilayer square lattice [32–37]. Because the sign problem is completely absent in the fully frustrated bilayer [29,30,32], we consider an extended model [26,38] defined by the Hamiltonian

$$H_{\text{ext}} = H + J_2 \sum_{\langle\langle\langle i,j \rangle\rangle\rangle} \vec{S}_i \cdot \vec{S}_j, \qquad (2)$$

in which the addition of the next-neighbor interdimer coupling, J_2, illustrated in Fig. 1, interpolates between the Shastry-Sutherland model at $J_2 = 0$ and the fully frustrated bilayer when J_2 and J are equal.

As we will show in Secs. III and IV, the thermodynamic properties of both models can be studied very accurately by QMC as long as the interdimer couplings, J and J_2, are not too large compared to J_D. As an aid to interpreting these results, we first obtain the full zero-temperature phase diagram of the extended model, H_{ext}, for which it is sufficient to consider $0 \leqslant J_2 \leqslant J$. We apply the variational tensor-network approach of infinite projected entangled pair states (iPEPS), the technical details of which we provide in Appendix A. This method has been shown previously [39] to provide very accurate results for the Shastry-Sutherland model [Eq. (1)], and in Fig. 2 we show the phase diagram of the extended model [Eq. (2)]. The ground state is clearly a dimer-singlet phase at small interdimer couplings and a square-lattice antiferromagnetic phase at large J; this latter phase becomes an effective $S = 1$ square-lattice antiferromagnet in the bilayer limit ($J_2/J = 1$) [32]. Only near the opposite (Shastry-Sutherland) limit does a small regime of a third phase appear, the intermediate "plaquette" phase (inset, Fig. 2) based on alternating squares of the J lattice [39–42]. The dimer and plaquette phases are gapped

TABLE I. Action of total-spin and spin-difference operator components on the local dimer-basis spin states. Because $\vec{T}_d^2$ and T_d^z are diagonal in this basis, we give only the eigenvalues for these operators. Note that in this basis D_d^z is not diagonal.

	$\vec{T}_d^2$	T_d^z	T_d^+	T_d^-	D_d^z	D_d^+	D_d^-
$\lvert S\rangle_d$	0	0	0	0	$\lvert 0\rangle_d$	$-\sqrt{2}\lvert +\rangle_d$	$\sqrt{2}\lvert -\rangle_d$
$\lvert 0\rangle_d$	2	0	$\sqrt{2}\lvert +\rangle_d$	$\sqrt{2}\lvert -\rangle_d$	$\lvert S\rangle_d$	0	0
$\lvert +\rangle_d$	2	1	0	$\sqrt{2}\lvert 0\rangle_d$	0	0	$-\sqrt{2}\lvert S\rangle_d$
$\lvert -\rangle_d$	2	-1	$\sqrt{2}\lvert 0\rangle_d$	0	0	$\sqrt{2}\lvert S\rangle_d$	0

and all phase transitions are first-order. We comment that a previous investigation [38] came to very similar conclusions, except that it missed the intermediate plaquette phase.

With a view to our QMC calculations, we next define the sign-problem-free Hamiltonian corresponding to the extended spin model of Eq. (2). Working in the dimer basis, we change the signs of the off-diagonal matrix elements in such a way that all of them are nonpositive. For a given dimer (J_D) bond, d, we combine the two spins that form this dimer, $\vec{S}_{d,1}$ and $\vec{S}_{d,2}$, to introduce the total-spin operator, $\vec{T}_d = \vec{S}_{d,1} + \vec{S}_{d,2}$, and the spin-difference operator, $\vec{D}_d = \vec{S}_{d,1} - \vec{S}_{d,2}$. In defining $\vec{D}_d$, it is necessary to fix a convention regarding the assignment of the spin labels 1 and 2, and here we allocate $\vec{S}_{d,1}$ to the left (lower) spin on a horizontal (vertical) dimer in Fig. 1(a). By considering the local spin-singlet and -triplet states on dimer d,

$$\lvert S\rangle_d = \tfrac{1}{\sqrt{2}}(\lvert\uparrow\downarrow\rangle_d - \lvert\downarrow\uparrow\rangle_d),$$
$$\lvert 0\rangle_d = \tfrac{1}{\sqrt{2}}(\lvert\uparrow\downarrow\rangle_d + \lvert\downarrow\uparrow\rangle_d), \qquad (3)$$
$$\lvert +\rangle_d = \lvert\uparrow\uparrow\rangle_d, \quad \lvert -\rangle_d = \lvert\downarrow\downarrow\rangle_d,$$

we summarize the action of the total-spin and spin-difference operators in Table I, where we use the conventional definitions $T_d^\pm = T_d^x \pm i T_d^y$ and $D_d^\pm = D_d^x \pm i D_d^y$.

The Hamiltonian H_{ext} [Eq. (2)] consists of (i) a sum of the separate local couplings, i.e., J_D, within each dimer d, which one may denote H_d, and (ii) sums over the interdimer terms, with couplings J and J_2, that connect two neighboring orthogonal dimers. The local contribution may be expressed as $H_d = \tfrac{1}{2}\vec{T}_d^2 - \tfrac{3}{4}$, i.e., in terms only of total-spin operators. The interdimer coupling for the two dimers d and d' indicated in Fig. 1(a) takes the form

$$H_{dd'} = \tfrac{1}{2}(J + J_2)\vec{T}_d \cdot \vec{T}_{d'} - \tfrac{1}{2}(J - J_2)\vec{T}_d \cdot \vec{D}_{d'}. \qquad (4)$$

Clearly, in the special case $J_2 = J$, the TD-coupling terms vanish, and in this limit, which corresponds to the fully frustrated bilayer model, QMC simulations formulated in the spin-dimer basis can be performed with no sign problem [28–32] despite the extreme frustration. By contrast, whenever $J_2 \neq J$, a finite TD-term is present in addition to the TT-terms, and in particular for the Shastry-Sutherland model ($J_2 = 0$) it is strong. This term leads to the reappearance of a minus-sign problem in the dimer basis, and in Sec. III we examine its severity in detail.

To complete the construction of the sign-problem-free Hamiltonian, $\widetilde{H}$, we start from H_{ext} and change the signs of
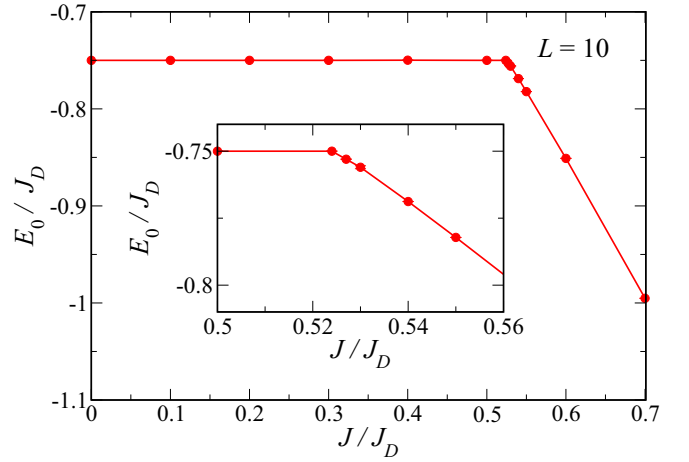

FIG. 3. Ground-state energy per dimer of the sign-problem-free model, $\widetilde{H}$, extracted from QMC simulations. The kink at $J/J_D = 0.526(1)$ signals a level-crossing out of the dimer singlet-product state.

all positive off-diagonal matrix elements in the dimer basis. The resulting interdimer exchange terms can be expressed most explicitly in terms of transfer operators within the basis of two-dimer states. As an example, the off-diagonal components of $\widetilde{H}$ contributed by the TD-terms are given by

$$\widetilde{H}_{dd'}^{\text{TD,off}} = -\tfrac{1}{2}\lvert J - J_2\rvert [\lvert +S\rangle\langle +0\rvert + \lvert +0\rangle\langle +S\rvert$$
$$+ \lvert +-\rangle\langle 0S\rvert + \lvert 0+\rangle\langle +S\rvert$$
$$+ \lvert +S\rangle\langle 0+\rvert + \lvert 0S\rangle\langle +-\rvert$$
$$+ (+ \leftrightarrow -)],$$

where the notation $\lvert S+\rangle$ denotes $\lvert S\rangle_d \otimes \lvert +\rangle_{d'}$ and the form is readily obtained with the help of Table I. The full sign-problem-free Hamiltonian in the dimer basis is the sum of the diagonal part, H_d, and the contributions from all such off-diagonal interdimer terms with their signs set to be nonpositive.

Because this Hamiltonian has no minus-sign problem by construction, it can be studied down to very low temperatures by QMC. The ground-state energy per dimer, E_0, for $\widetilde{H}$ is shown in Fig. 3. As expected, the ground state for weak interdimer coupling is the product of singlets on all dimer bonds, of course with energy $-\tfrac{3}{4}J_D$ per dimer. As in the Shastry-Sutherland model, this product state remains as the exact ground state up to a fixed, finite value of the interdimer coupling, which we find to be $J = 0.526(1)J_D$ when $J_2 = 0$. At that coupling ratio, a level crossing takes place, signaling a first-order transition to another phase. Because this model is not physical, but useful only to discuss QMC simulations of the extended Shastry-Sutherland model, we have not tried to understand the precise nature of the high-J phase of $\widetilde{H}$. We note only that it appears to extend up to very large J/J_D with no sign of a further transition, but given the complicated form of the model we do not speculate on the physics in this regime.

By contrast, at small interdimer coupling, it is straightforward to convince oneself that the ground state of the sign-problem-free Hamiltonian must be the same as that of the Shastry-Sutherland model. First, we observe that the

singlet-product state is an element of the dimer basis in which the Hamiltonian is formulated. Thus, the fact that it is an eigenstate of the Shastry-Sutherland model implies that all off-diagonal matrix elements involving that state must vanish. Because passing from the Shastry-Sutherland model to the sign-problem-free Hamiltonian involves only changing the signs of the positive off-diagonal matrix elements, all off-diagonal matrix elements involving the singlet-product state will still vanish in $\widetilde{H}$, implying that this state is an eigenstate of that Hamiltonian. Second, this state is clearly the ground state of the model with vanishing off-diagonal matrix elements, and it is separated from the first excited state by an energy equal to the intradimer coupling. A simple perturbative argument therefore implies that this situation has to remain true over a finite regime of parameter space where the off-diagonal matrix elements are small compared to the intradimer coupling.

Closing this section with a brief technical summary, we perform stochastic series expansion [43] QMC simulations in the dimer basis [28,29] with directed loop updates [44,45] to compute the thermodynamic properties of the Shastry-Sutherland model [Eq. (1)] and to characterize the sign problem in the extended model [Eq. (2)]. These simulations perform an unrestricted sampling of the configuration space, meaning one not constrained to any subset of the Hilbert space defined by the S^z and D^z operators of the total system. We deploy a parallel tempering approach [28] to enhance state mixing, which is particularly important near the limit of the fully frustrated bilayer. We access system sizes $N = 2 \times L \times L$ up to $L = 10$ and temperatures as low as $T = 0.01 J_D$ where the sign problem is mild. Where the sign problem is severe, we have worked down to average-sign values $\langle \text{sign} \rangle' = 0.06$, where it is necessary to compensate by increasing the QMC sampling (the CPU time) by a factor of nearly 300.

III. THE MINUS SIGN

Turning now to the minus sign in the model of Eq. (2), it is always possible to simulate a model with a sign problem using QMC, by taking the absolute values of the weights, $|W_c|$, of each configuration c from the corresponding sign-problem-free model. In this procedure, the average of any observable, A, is the ratio of the averages of the observable and of the sign [46,47],

$$\langle A \rangle = \frac{\sum_c W_c A_c}{\sum_c W_c} = \frac{\sum_c \text{sign}(W_c)|W_c|A_c}{\sum_c \text{sign}(W_c)|W_c|} = \frac{\langle \text{sign} A \rangle'}{\langle \text{sign} \rangle'}. \quad (5)$$

Here the notation $\langle X \rangle'$ indicates that $|W_c|$ is obtained from the sign-problem-free Hamiltonian, in which the weights are readily sampled, but we stress that the physics of the original model is contained in the signs, $\text{sign}(W_c) = W_c/|W_c|$, of every configuration c, which appear in both the numerator and the denominator of $\langle A \rangle$. In a typical frustrated quantum spin model, this approach can no longer be used when the temperature becomes low compared to the energy scales set by the coupling strengths, because then the average sign, $\langle \text{sign} \rangle'$ in the denominator of Eq. (5), tends to zero, inducing error bars larger than the signal.

The central result of the present contribution is reported in Fig. 4. While $\langle \text{sign} \rangle'$ for the Shastry-Sutherland model does
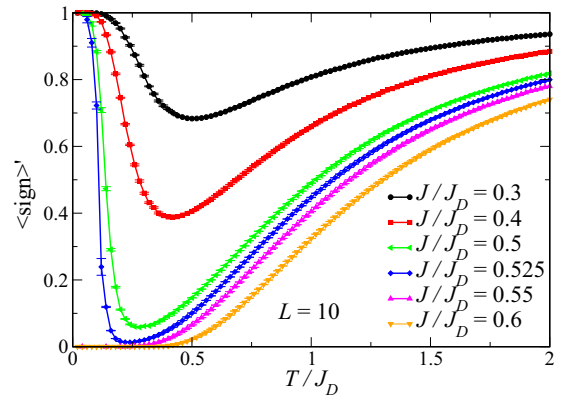

FIG. 4. Temperature dependence of the average sign, $\langle \text{sign} \rangle'$, computed for the Shastry-Sutherland model [Eq. (1)] with different values of the coupling ratio.

indeed become small at temperatures below J_D, it increases again at low temperatures and recovers to a value of precisely 1 at zero temperature. This behavior occurs provided that the ground state of the sign-problem-free model is the singlet-product state, and thus it holds up to the coupling ratio $J/J_D = 0.526(1)$. Above that coupling value, the behavior of $\langle \text{sign} \rangle'$ is typical of any general model with a minus sign, i.e., the average becomes very small and never increases again [46,47].

The fact that the average sign goes rigorously to 1 at zero temperature is a simple consequence of the fact that both the Shastry-Sutherland model and its sign-problem-free counterpart have the same ground state. Then the denominator of Eq. (5) is strictly equal to 1 and the average of any quantity is its ground-state expectation value. This should be contrasted with the frustrated ladder away from perfect frustration, where the ground state cannot be expressed exactly in the dimer basis and periodic boundary conditions introduce components with a minus sign [31]. In that case, the average sign also increases again as the temperature is lowered, but recovers only to a value close, i.e., not exactly equal, to 1.

Our motivation for considering the extended Shastry-Sutherland model of Eq. (2) was that the limit ($J_2 = J$) of the fully frustrated bilayer is completely sign-problem-free. One may therefore hope that a significant fraction of the phase diagram of Fig. 2, in the regime around this limit, may have only a mild sign problem and would thus be amenable to QMC. To investigate this possibility, we have calculated $\langle \text{sign} \rangle'$ for the extended model by working on a system of fixed size $L = 10$ and at a fixed temperature $T = 0.1 J_D$. As Fig. 5 makes clear, the average sign is essentially equal to 1 in a large portion of the singlet-product phase. The border of the sign-problem-free region is almost vertical near the Shastry-Sutherland limit (small J_2), which is a consequence of the phase transition at $J/J_D = 0.526$ in the (unphysical) sign-problem-free model, as discussed in Sec. II and Fig. 3. For J_2 values beyond approximately $0.5 J$, the boundary of the sign-problem-free region matches quite accurately the physical boundary to the antiferromagnetic phase, which we show in Fig. 5 by reproducing the transition line from the ground-state phase diagram computed by iPEPS (Fig. 2). In the fully
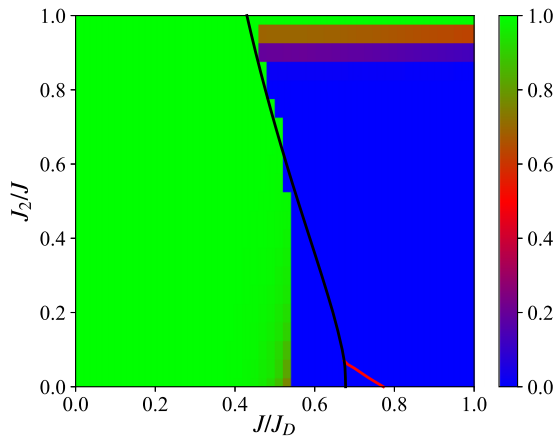
FIG. 5. Average sign, $\langle sign \rangle'$, computed at a temperature $T = 0.1 J_D$ throughout the phase diagram of the extended Shastry-Sutherland model [Eq. (2)] for a system of 10×10 dimers. Solid lines reproduce the phase boundaries computed by iPEPS and shown in Fig. 2.

frustrated limit, $\langle sign \rangle'$ exhibits no transition, which is to be expected because the physical model is completely free of any sign problems here [29,30,32]. However, the sign problem manifestly grows very rapidly with "detuning" ($J_2 \neq J$) away from the fully frustrated line, leaving very little additional parameter space where one might hope to use QMC to study, for example, the dimerized-to-antiferromagnetic phase transition. We comment that, in the regime of a dominant interaction J, where the ground state of the Shastry-Sutherland model [Eq. (1)] is antiferromagnetically ordered (right side of Fig. 2), one may perform sign-problem-free QMC simulations in the standard basis of spin configurations only for $J_D = 0$. For any finite values $J_D > 0$, these simulations are again plagued by a severe sign problem, which prevents us from examining the transition regime out of the antiferromagnetic phase.

IV. THERMODYNAMIC CALCULATIONS

For our calculations of thermodynamic properties, we focus on the original Shastry-Sutherland model of Eq. (1), i.e., the case $J_2 = 0$ in Eq. (2). By inspection of Fig. 4, the average sign for a coupling ratio such as $J/J_D = 0.5$ falls (in calculations using $L = 10$) to values as low as 0.06 over a significant range of intermediate temperatures. Nonetheless, as a consequence of our observations concerning the ground state (Sec. II) and the minus sign (Sec. III), it remains possible to obtain very accurate results in the regime $J \lesssim 0.5 J_D$ for the magnetic specific heat, $C(T)$, and susceptibility, $\chi(T)$, which are shown, respectively, in Figs. 6(a) and 6(b).

Figure 6 shows data obtained by simulations for clusters of 10×10 dimers, corresponding to a system containing $N = 200$ $S = 1/2$ spins. In this regime, finite-size effects are sufficiently small that these results can be considered as fully representative of the thermodynamic limit. For this reason, we have not performed simulations for still larger values of N, although this would be completely feasible due to the rather mild sign problem in this parameter regime. In the limit $J = 0$, we recover the result for decoupled dimers, which is known analytically [28,48–50] and is represented by the
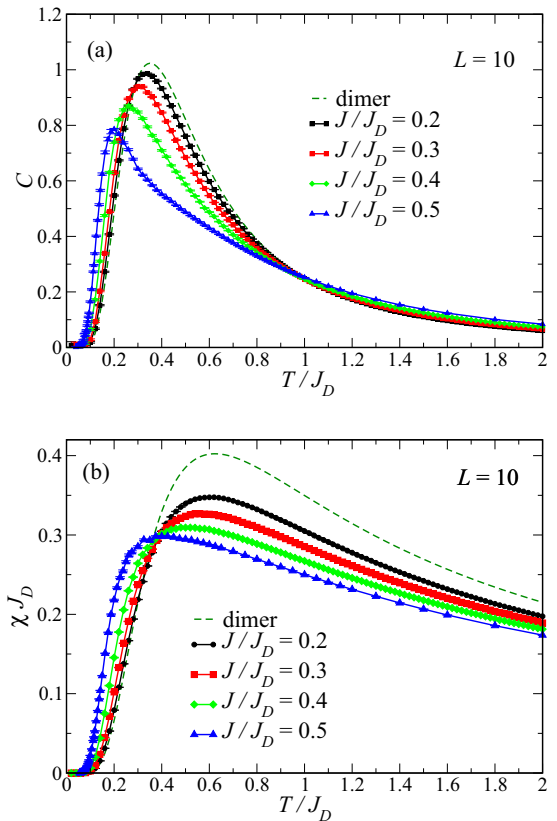

FIG. 6. (a) Magnetic specific heat, $C(T)$, and (b) susceptibility, $\chi(T)$, of the Shastry-Sutherland model computed by QMC for systems of size $L = 10$, shown per dimer for different values of the coupling ratio.

dashed lines. As the ratio J/J_D is increased, $\chi(T)$ shows a flattening of its maximum accompanied by a downward shift of its low-temperature flank [Fig. 6(b)], indicating a decreasing spin gap. $C(T)$ exhibits a similar suppression of both spin gap and peak position [Fig. 6(a)]; although the full response remains broad in temperature, there is a distinct sharpening of the low-temperature peak as J/J_D approaches 0.5.

In Fig. 7, we study the challenging regime of coupling ratios between $J/J_D = 0.5$ and the transition from dimer to plaquette order. This is also the region of interest to experiment, for the description of $SrCu_2(BO_3)_2$. In addition to QMC data, here we also show ED results, obtained by full diagonalization of the relevant Hamiltonians for clusters of $N = 20$ spins, and the results of interpolated high-temperature series expansions (HTSEs); technical details of the HTSE approach may be found in Appendix B. Figures 7(a) and 7(b) revisit $C(T)$ and $\chi(T)$ for the case $J/J_D = 0.5$ to compare our $N = 200$ QMC data (Fig. 6) with results for $N = 32$. The negligible deviations between the two data sets confirm that $N = 200$ is indeed well in the thermodynamic limit (whence, again, we did not perform simulations for any larger N, although this would still be possible at $J/J_D = 0.5$). However, minor deviations from the $N = 20$ ED data do start to become visible around the maximum of the specific heat, indicating the onset of finite-size effects for $N \leqslant 20$ at $J \geqslant 0.5 J_D$.
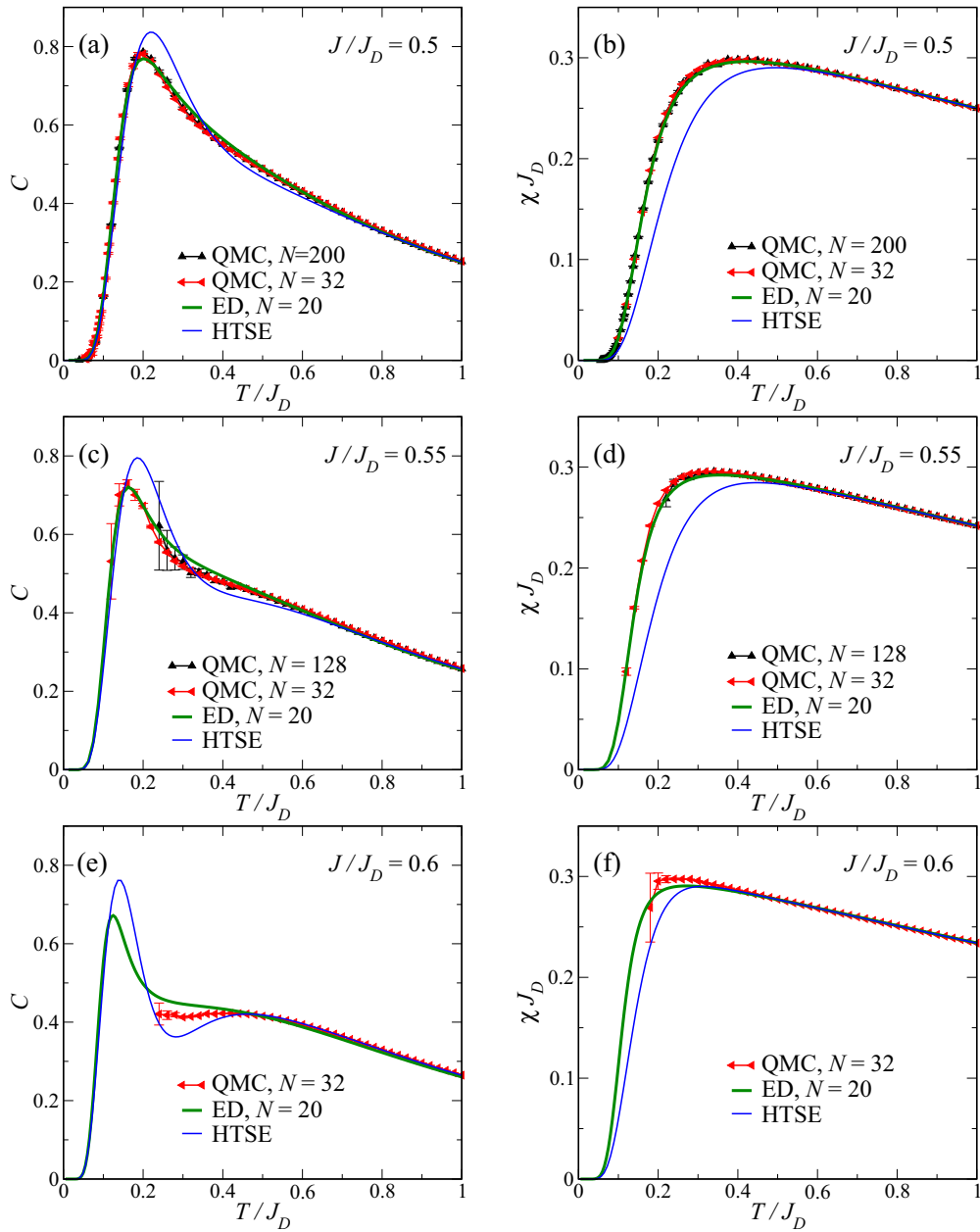
FIG. 7. (a), (c), (e) Magnetic specific heat, $C(T)$, and (b), (d), (f) susceptibility, $\chi(T)$, of the Shastry-Sutherland model computed by QMC and shown per dimer for the largest system sizes feasible at coupling ratios $J/J_D = 0.5$ (a,b), 0.55 (c), (d), and 0.6 (e), (f).

Turning to our HTSE calculations, the interpolated tenth-order HTSEs capture the qualitative behavior visible in the QMC and ED data for $J/J_D = 0.5$ and improve upon previous seventh-order studies [26], most notably in that the interpolation scheme outlined in Appendix B enhances the stability of the expansion in comparison to earlier work. However, in contrast to the situation at smaller values of J/J_D (Appendix B), our HTSEs are not able to reproduce the QMC and ED results for $J/J_D = 0.5$ with quantitative accuracy. With a view to understanding the limits of the present procedure, we note that the low-temperature edge of $C(T)$, which is normally controlled by the spin gap, is reproduced very well in Fig. 7(a), whereas this is not the case for $\chi(T)$ in Fig. 7(b). Technically, a possible reason why $C(T)$ is relatively better behaved may lie in the additional energy and entropy sum

rules that can be used to stabilize the interpolation [51–53]. Physically, one may suspect this discrepancy of indicating the onset of a regime where the low-temperature thermodynamics are no longer controlled in a conventional way by a small number of low-lying excited states [28], and we return to this point below.

At $J/J_D = 0.55$ and 0.6, the average sign in the Shastry-Sutherland model no longer recovers to 1 at low temperatures [Fig. 4]. Unsurprisingly, dimer-basis QMC simulations become very much more challenging in this regime and we are forced to reduce the system size to reach meaningfully low temperatures. System sizes of $N = 32$ are required to reach temperatures below the maximum of the specific heat at $J = 0.55 J_D$ [Fig. 7(c)], but comparison with $N = 128$ data does indicate that $N = 32$ remains sufficient to keep deviations
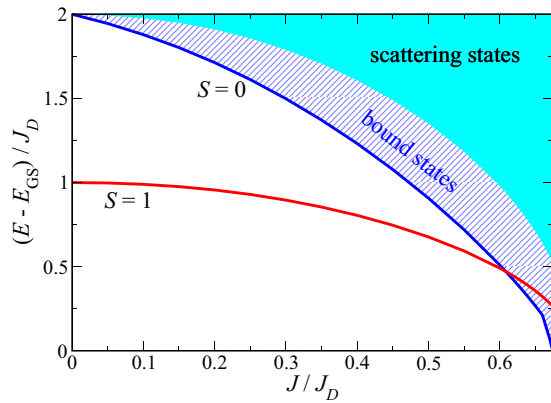
FIG. 8. Schematic representation of the excitation spectrum of the Shastry-Sutherland model shown as a function of coupling ratio, based on ED calculations using a cluster of $N = 36$ spins. Energies are measured with respect to the ground-state energy, $E_{GS} = -\frac{3}{8}N J_D$. Solid lines denote the gaps to the lowest triplet ($S = 1$, red) and singlet ($S = 0$, blue) excited states. The bandwidth of the one-particle triplet excitations is approximately the thickness of the red line. The hatched region represents continua of dispersive $S = 0$ and $S = 1$ two-particle bound states. The shaded region, whose lower boundary is given by twice the triplet gap, indicates the regime where many-particle scattering continua are allowed.

from the thermodynamic limit within the statistical error bars. By contrast, ED results for $N = 20$ at $J = 0.55 J_D$ show definite finite-size effects, specifically in the region $0.2 < T/J_D < 0.4$ in $C(T)$ and around the maximum of $\chi(T)$. The coupling ratio $J/J_D = 0.6$, shown in Figs. 7(e) and 7(f), marks the outer limit of the regime where the low-temperature behavior of the Shastry-Sutherland model can be considered to be under control in any quantitative sense. Comparison between $N = 20$ ED and $N = 32$ QMC data shows that $C(T)$ [Fig. 7(e)] remains subject to very significant finite-size effects for $T/J_D \lesssim 0.5$, where it is possible that nonmonotonic behavior sets in, while it is difficult to benchmark anything below the maximum of $\chi(T)$ [Fig. 7(f)].

The results of Fig. 7 confirm the physical trends observed in Fig. 6, namely the downward shift of the low-temperature rise in both $C(T)$ and $\chi(T)$ with increasing J/J_D, accompanied by a flattening of the maximum in $\chi(T)$ and a sharpening of the peak in $C(T)$. The emergence of this distinctive maximum at a temperature scale very low in comparison with the coupling constants constitutes the dominant thermodynamic feature as one approaches the first-order transition from the dimer-singlet to the plaquette phase at $J/J_D \approx 0.675$ [39]. This behavior is analogous to that observed on approaching the boundary of the rung-singlet phase in highly frustrated spin ladders [28,31], where its origin was traced to the presence of many low-lying bound rung-triplet excitations. Our results suggest that the same type of bound-state mechanism is at work in the less constrained 2D system, and that the emergence of the low-temperature maximum in the specific heat is its clearest thermodynamic fingerprint.

To expand upon this point, in Fig. 8 we show a schematic representation of the excitation spectrum of the Shastry-Sutherland model in the thermodynamic limit as a function

of J/J_D. The solid red and blue lines mark, respectively, the gaps to the lowest-lying triplet and singlet states, which we have extracted from earlier $N = 36$ ED calculations [16]; the former have their origin in single dimer-triplet excitations, which are only very weakly dispersive, and the latter in bound pairs of dimer triplets. We note that the decrease in energy not only of the spin gap but also of the two-particle bound states on increasing J/J_D is already well documented [25,27,54,55]. A considerable number of dispersive singlet and triplet bound states remains below the edge of the two-particle continuum [27], as represented by the blue hatched region in Fig. 8. We draw attention in particular to the fact that the gap of the lowest singlet mode decreases faster with coupling ratio than the triplet gap, until the two cross at $J/J_D \approx 0.61$ on the $N = 36$ cluster. While the singlet spectrum remains unknown in detail, it is likely that these bound states are responsible for the sharpening peak in $C(T)$ at $J/J_D \gtrsim 0.6$. The fact that the gap of the lowest singlet bound state for $N = 36$ closes very near the boundary of the dimer singlet-product phase, $J/J_D \approx 0.675$ [39] (right border of Fig. 8), is expected to indicate the crossing of levels occurring at the first-order transition to the plaquette phase.

A more detailed analysis of the evolution with J/J_D of the n-particle bound states in the ED spectrum with $n > 2$ is an involved problem that we defer to a future study. We stress that, over most of the singlet-product regime of the phase diagram, and certainly the range $J/J_D \leqslant 0.5$, the thermodynamic response of the Shastry-Sutherland model (Fig. 6) should be characteristic of just one gap, that to the lowest triplet. Only beyond this region, coincidentally in the zone where QMC becomes dramatically more difficult [Figs. 7(c)-7(f)], might the proximity of the lowest singlet state(s) indeed begin to play a role (Fig. 8).

V. CONCLUSIONS AND PERSPECTIVES

We have shown that, even for models where QMC simulations suffer from a minus-sign problem, it may be possible to obtain extremely accurate results for the low-temperature thermodynamics. A sufficient condition is that the ground states of the physical model and of the corresponding sign-problem-free model, constructed by making all off-diagonal matrix elements nonpositive, be the same. This condition has allowed us to compute numerically exact results for the magnetic specific heat and susceptibility of the Shastry-Sutherland model throughout the parameter range where the ratio of the inter- to intradimer couplings is less than or equal to 0.526(1).

This is the regime of coupling ratios where the ground state of both models is a product of singlets on every dimer bond, the state about which Shastry and Sutherland constructed their Hamiltonian. With regard to the material realizing the Shastry-Sutherland model, it is of course unfortunate that this critical ratio for the success of QMC is smaller than the coupling ratio in $SrCu_2(BO_3)_2$ [9], which is believed to be approximately 0.63 [25]. Because the real Shastry-Sutherland model has, at this coupling ratio, not yet undergone the phase transition to the plaquette state, we are investigating possible modifications to the conventional sign-problem-free model introduced in Sec. II with a view toward making the weights sampled in this model applicable at coupling ratios larger than 0.526.

Our QMC results offer considerable perspective on other numerical approaches to the thermodynamics of the Shastry-Sutherland model. Clearly, finite-size effects become increasingly important at $J/J_D > 0.5$ and thus ED studies, particularly using clusters of $N \leqslant 20$ spins [19,24,25], must be interpreted with care at low temperatures and especially at $J/J_D \approx 0.63$. This highlights the importance of ED variants that access larger N by avoiding full diagonalization, such as that applied recently [56] to compute the thermodynamic properties of a kagome cluster with $N = 42$ $S = 1/2$ spins. We have also used our QMC results to benchmark some recent advances in HTSE approaches. While this comparison demonstrates qualitative progress, in that the problem of low-temperature divergences, which plagued previous HTSE implementations [19,26], can be overcome by suitable interpolation schemes, it shows at the quantitative level that HTSE for the Shastry-Sutherland model remains limited by the maximum accessible expansion order of ten. Consequently, the accuracy of our HTSEs remains below that of QMC and even small-system ED over the full phase diagram of the model. A combination of deriving higher-order series (the 17th order has been attained in a recent study [52] of the kagome lattice) and more refined interpolation schemes [51–53] may offer a competitive HTSE approach to the parameter regime relevant for $SrCu_2(BO_3)_2$.

Beyond the Shastry-Sutherland model, our results imply that QMC simulations should be possible for any frustrated model whose ground state is known exactly, provided that the Hamiltonian matrix can be expressed in a basis that contains this exact ground state. We anticipate that this observation will open up the field of QMC calculations of the thermodynamics for a range of frustrated quantum spin systems, most straightforwardly those constructed to possess exact dimer- and plaquette-product ground states. Here we have explored the extension of the Shastry-Sutherland model to the limit of the fully frustrated bilayer, where the sign problem is entirely absent, and demonstrate by comparison with iPEPS calculations of the ground-state phase diagram how the extent of the sign problem can be understood.

ACKNOWLEDGMENTS

APPENDIX A: IPEPS CALCULATIONS

The ground-state phase diagram in Fig. 2 was obtained by means of a variational tensor-network ansatz known as iPEPS [57–59]. An iPEPS consists of a unit cell of local tensors that is repeated over the lattice. Each local tensor has one physical index which, for the present model, represents the two sites on a dimer, and four auxiliary indices that connect neighboring local tensors to form a square geometry in accord

with the lattice structure shown in Fig. 1(b). The auxiliary vector spaces have a dimension D, the bond dimension, which controls the accuracy of the ansatz, in that higher D values allow more entanglement to be captured by the iPEPS. All three of the phases in Fig. 2 can be represented by an iPEPS with a two-sublattice unit cell consisting of two local tensors (four sites).

We compute physical expectation values using a variant [60] of the corner-transfer-matrix algorithm [61,62]. The corner matrices have their own boundary bond dimension, χ, which should be taken to be sufficiently large $(\chi(D) > D^2)$ that the error due to the use of finite χ is negligible compared to the error due to the finite value of D. To increase the efficiency of our calculations, we exploit the global U(1) symmetry of the model [63,64].

Given an initial iPEPS, we obtain an approximate ground state either by projecting the starting state using imaginary-time evolution or by direct minimization of the energy using the variational-update method of Ref. [65]. In the former approach, the projection operator is decomposed into a series of two-body gates. Application of a single gate increases the dimension of the bond connecting the two tensors in question, which then has to be truncated back to D. This process may be performed using the simple-update method [66], in which the truncation of a bond index is based on a local approximation of the state, or by the more accurate but computationally more expensive full-update algorithm [59,67,68], where the entire many-body state is taken into account for the truncation.

To construct the phase diagram shown in Fig. 2, we employed simple-update calculations at a fixed bond dimension $D = 10$, which already provide a good estimate of the phase boundaries in the limit of infinite D, as we show below. We computed the transition points along several horizontal and vertical cuts through the phase diagram. Working at a fixed value of J_2/J for a horizontal cut, the critical coupling J_c/J_D was determined by locating the intersection point where the energies of states initialized in the two adjacent phases intersect (making use of the hysteresis in the vicinity of a first-order phase transition). We note that, because the ground-state energy in the dimer singlet-product phase is known exactly, the fixed-D estimate of the phase boundary between this dimer phase and either of the other phases (antiferromagnetic or plaquette) shifts to smaller values of J/J_D with increasing D.

To determine the accuracy of the fixed-D simple-update phase diagram, we have executed additional variational-update calculations followed by extrapolations to the $D \rightarrow \infty$ limit, where our results should be exact, along several cuts in the parameter space. Extrapolations in this case were performed on the basis of the truncation error [69]. By comparison with the $D = 10$ simple-update phase boundaries along four horizontal cuts, taken at $J_2/J = 0.25$, 0.50, 0.75, and 1.00, we observe that the phase boundary for the transition from the singlet-product to the antiferromagnetic state, displayed in Fig. 2, agrees with the variational-update $D \rightarrow \infty$ phase boundary up to the first four digits. The uncertainty in the phase boundaries of the plaquette phase is somewhat larger, and is represented by the error bars on three of the points shown in Fig. 9, which were obtained from detailed studies along two horizontal cuts at $J_2/J = 0$ and a vertical
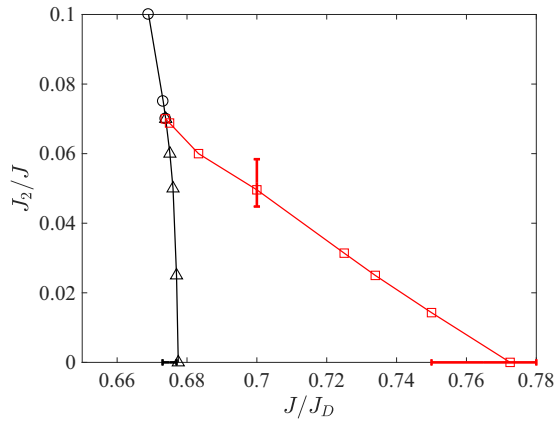
FIG. 9. Phase boundaries obtained by simple-update iPEPS calculations. The error bars illustrated for three data points are representative of all others. These were obtained from extrapolated $(D \to \infty)$ full-update calculations at $J_2/J = 0$ and from variational-update calculations at $J/J_D = 0.7$. Results for $J_2/J = 0$ were taken from Ref. [39].

FIG. 10. (a) Magnetic specific heat, $C(T)$, and (b) susceptibility, $\chi(T)$, of an isolated spin-1/2 dimer, shown for comparison with the interpolated tenth-order HTSE result.

cut at $J/J_D = 0.7$. We comment that the error bars for the transition from the plaquette to the antiferromagnetic phase are the largest because this transition appears to be only weakly first-order. The thickness of the lines marking the phase boundaries in Fig. 2 was determined on the basis of the error bars shown in Fig. 9.

APPENDIX B: INTERPOLATION OF HIGH-TEMPERATURE SERIES EXPANSIONS

As its name implies, the aim of a HTSE is to express the magnetic susceptibility and specific heat in powers of the inverse temperature,

$$\chi(T) = \sum_{n=0}^{M} \chi_n T^{-n}, \quad C(T) = \sum_{n=0}^{M} C_n T^{-n}, \quad \text{(B1)}$$

to obtain results exact in the high-T limit and systematic approximations elsewhere. We began our study by using the methods and code described in Ref. [70] to generate series to order $M = 10$ for $\chi(T)$ and $C(T)$ in the Shastry-Sutherland model. However, the truncated bare series of Eq. (B1) diverge in the low-temperature regime, which is the focus of the present study. The conventional solution to this divergence is the use of Padé approximants (reviewed in Ref. [71]), but this approach is completely unsuitable here because it always yields a power-law low-temperature behavior, rather than the exponentially activated behavior characteristic of a gapped model (Sec. IV).

Thus we adopt a simple approach to constructing an interpolation scheme, which is to exchange variables to work with an expansion in terms of exponential functions, $e^{-\Delta/T}$, containing a gap parameter Δ. We comment that several similar but more sophisticated schemes have been proposed recently [51–53]. Here we take the additional step of incorporating the
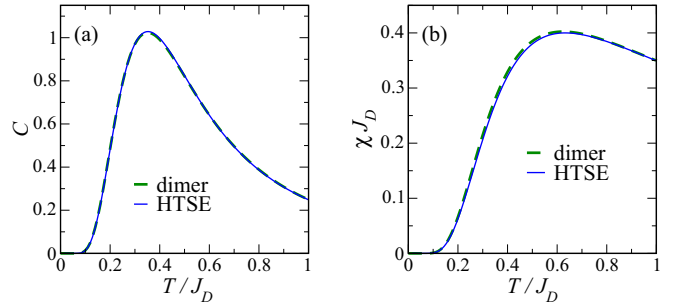
known leading high-temperature asymptotics into the ansatz to obtain

$$\chi_T(T) = \frac{1}{T} \sum_{n=1}^{M_\chi} \tilde{\chi}_n \, e^{-n\,\Delta/T}, \quad \text{(B2)}$$

$$C_T(T) = \frac{1}{T^2} \sum_{n=1}^{M_C} \tilde{C}_n \, e^{-n\,\Delta/T}. \quad \text{(B3)}$$

Because the exponential functions within the sum decay faster than any power law, the expressions Eqs. (B2) and (B3) have well-defined low-temperature behavior and tend to zero as $T \to 0$. The coefficients $\tilde{\chi}_n$ and $\tilde{C}_n$ may be determined by demanding that the Taylor expansions of Eqs. (B2) and (B3) match the corresponding coefficients in Eq. (B1).

For the susceptibility, indeed we determine the $M_\chi = M$ coefficients $\tilde{\chi}_n$ in this manner. For the specific heat, we can obtain additional constraints, following Refs. [51–53], by further imposing two sum rules, one for the ground-state energy,

$$E_0 = -\int_0^\infty dT \, C(T), \quad \text{(B4)}$$

and one for the total entropy per dimer of a spin-1/2 system,

$$\int_0^\infty dT \, \frac{C(T)}{T} = 2 \ln 2. \quad \text{(B5)}$$

Performing the relevant integrals in Eq. (B3) yields the two additional linear equations

$$\sum_{n=1}^{M_C} \frac{\tilde{C}_n}{n\,\Delta} = -E_0 \quad \text{and} \quad \sum_{n=1}^{M_C} \frac{\tilde{C}_n}{(n\,\Delta)^2} = 2 \ln 2, \quad \text{(B6)}$$

constraining the $M_C = M + 1$ coefficients $\tilde{C}_n$. We comment that the respective relations between the coefficients χ_n, C_n and $\tilde{\chi}_n$, $\tilde{C}_n$ are highly nontrivial. In particular, the individual coefficients $\tilde{\chi}_n$ and $\tilde{C}_n$ are not constrained to converge when $M \to \infty$, i.e., the entire procedure should be considered only as an interpolation between the low- and high-temperature limits using a finite-order approximation to the latter.

This interpolation procedure makes use of two additional parameters. One is the ground-state energy per dimer unit cell, which, as noted in Sec. II, is known exactly for the Shastry-Sutherland model in its singlet-product state [7],

namely $E_0 = -\frac{3}{4} J_D$. The other is a value for the gap at any given coupling ratio J/J_D, and in our present HTSE studies we have used the values of the gap obtained by ED for the $N = 36$ cluster, which are shown in Fig. 8. We comment again that for $J/J_D \lesssim 0.6$ the lowest excitation is indeed the one-particle triplet mode, and thus that no distinction is required between the gaps used for the susceptibility and specific-heat expansions.

We illustrate the efficacy of the HTSE interpolation procedure by using the example of the isolated dimer, i.e., the case $J = 0 = J_2$ in Eq. (2). Exact results for $\chi(T)$ and $C(T)$ of a single dimer are known analytically [28,48–50], and in fact

one may observe explicitly that low-temperature expansions of the exact expressions correspond precisely to the ansatz used in Eqs. (B2) and (B3). Figure 10 compares these exact results for $\chi(T)$ and $C(T)$, shown already in Fig. 6, with the interpolated tenth-order HTSE. Although the overall level of agreement could be classified as excellent, some deviations can be observed upon close inspection. We remark that, even in the isolated-dimer limit, the energy and entropy sum rules [Eqs. (B6)] are essential to stabilize the interpolation of $C(T)$ at lower temperatures, most notably around its maximum. In $\chi(T)$, which is less well constrained, minor deviations are evident in the temperature scale [cf. Figs. 7(b), 7(d), and 7(f)] as well as in the magnitude.

[1] J. Richter, J. Schulenburg, and A. Honecker, Quantum magnetism in two dimensions: From semi-classical Néel order to magnetic disorder, in *Quantum Magnetism*, edited by U. Schollwöck, J. Richter, D. J. J. Farnell, and R. F. Bishop (Springer, Berlin, 2004), pp. 85–153.

[2] L. Balents, Spin liquids in frustrated magnets, Nature **464**, 199 (2010).

[3] C. Lacroix, P. Mendels, and F. Mila, *Introduction to Frustrated Magnetism: Materials, Experiments, Theory*, Springer Series in Solid-State Sciences, Vol. 164 (Springer, Berlin, 2011).

[4] H. T. Diep, *Frustrated Spin Systems*, 2nd ed. (World Scientific, Singapore, 2013).

[5] J.-K. Kim and M. Troyer, Low Temperature Behavior and Crossovers of the Square Lattice Quantum Heisenberg Antiferromagnet, Phys. Rev. Lett. **80**, 2705 (1998).

[6] K. Harada, M. Troyer, and N. Kawashima, The two-dimensional $S = 1$ quantum Heisenberg antiferromagnet at finite temperatures, J. Phys. Soc. Jpn. **67**, 1130 (1998).

[7] B. S. Shastry and B. Sutherland, Exact ground state of a quantum mechanical antiferromagnet, Physica B+C **108**, 1069 (1981).

[8] H. J. Liao, Z. Y. Xie, J. Chen, Z. Y. Liu, H. D. Xie, R. Z. Huang, B. Normand, and T. Xiang, Gapless Spin-Liquid Ground State in the $S = 1/2$ Kagome Antiferromagnet, Phys. Rev. Lett. **118**, 137202 (2017).

[9] H. Kageyama, K. Yoshimura, R. Stern, N. V. Mushnikov, K. Onizuka, M. Kato, K. Kosuge, C. P. Slichter, T. Goto, and Y. Ueda, Exact Dimer Ground State and Quantized Magnetization Plateaus in the Two-Dimensional Spin System SrCu$_2$(BO$_3$)$_2$, Phys. Rev. Lett. **82**, 3168 (1999).

[10] K. Onizuka, H. Kageyama, Y. Narumi, K. Kindo, Y. Ueda, and T. Goto, 1/3 magnetization plateau in SrCu$_2$(BO$_3$)$_2$ - stripe order of excited triplets -, J. Phys. Soc. Jpn. **69**, 1016 (2000).

[11] K. Kodama, M. Takigawa, M. Horvatić, C. Berthier, H. Kageyama, Y. Ueda, S. Miyahara, F. Becca, and F. Mila, Magnetic superstructure in the two-dimensional quantum antiferromagnet SrCu$_2$(BO$_3$)$_2$, Science **298**, 395 (2002).

[12] S. E. Sebastian, N. Harrison, P. Sengupta, C. D. Batista, S. Francoual, E. Palm, T. Murphy, N. Marcano, H. A. Dabkowska, and B. D. Gaulin, Fractalization drives crystalline states in a frustrated spin system, Proc. Natl. Acad. Sci. USA **105**, 20157 (2008).

[13] M. Takigawa and Frédéric Mila, Magnetization plateaus, in *Introduction to Frustrated Magnetism: Materials, Experiments,*

Theory, edited by C. Lacroix, P. Mendels, and F. Mila (Springer, Berlin, 2011), pp. 241.

[14] M. Takigawa, M. Horvatić, T. Waki, S. Krämer, C. Berthier, F. Lévy-Bertrand, I. Sheikin, H. Kageyama, Y. Ueda, and F. Mila, Incomplete Devil's Staircase in the Magnetization Curve of SrCu$_2$(BO$_3$)$_2$, Phys. Rev. Lett. **110**, 067210 (2013).

[15] M. Jaime, R. Daou, S. A. Crooker, F. Weickert, A. Uchida, A. E. Feiguin, C. D. Batista, H. A. Dabkowska, and B. D. Gaulin, Magnetostriction and magnetic texture to 100.75 Tesla in frustrated SrCu$_2$(BO$_3$)$_2$, Proc. Natl. Acad. Sci. USA **109**, 12404 (2012).

[16] Y. H. Matsuda, N. Abe, S. Takeyama, H. Kageyama, P. Corboz, A. Honecker, S. R. Manmana, G. R. Foltin, K. P. Schmidt, and F. Mila, Magnetization of SrCu$_2$(BO$_3$)$_2$ in Ultrahigh Magnetic Fields up to 118 T, Phys. Rev. Lett. **111**, 137204 (2013).

[17] S. Haravifard, D. Graf, A. E. Feiguin, C. D. Batista, J. C. Lang, D. M. Silevitch, G. Srajer, B. D. Gaulin, H. A. Dabkowska, and T. F. Rosenbaum, Crystallization of spin superlattices with pressure and field in the layered magnet SrCu$_2$(BO$_3$)$_2$, Nat. Commun. **7**, 11956 (2016).

[18] M. Albrecht and F. Mila, First-order transition between magnetic order and valence bond order in a 2D frustrated Heisenberg model, Europhys. Lett. **34**, 145 (1996).

[19] S. Miyahara and K. Ueda, Exact Dimer Ground State of the Two Dimensional Heisenberg Spin System SrCu$_2$(BO$_3$)$_2$, Phys. Rev. Lett. **82**, 3701 (1999).

[20] C. K. Majumdar and D. K. Ghosh, On next-nearest-neighbor interaction in linear chain. I, J. Math. Phys. **10**, 1388 (1969).

[21] C. K. Majumdar and D. K. Ghosh, On next-nearest-neighbor interaction in linear chain. II, J. Math. Phys. **10**, 1399 (1969).

[22] C. K. Majumdar, Antiferromagnetic model with known ground state, J. Phys. C: Solid State Phys. **3**, 911 (1970).

[23] H. Kageyama, K. Onizuka, Y. Ueda, M. Nohara, H. Suzuki, and H. Takagi, Low-temperature specific heat study of SrCu$_2$(BO$_3$)$_2$ with an exactly solvable ground state, J. Exp. Theor. Phys. **90**, 129 (2000).

[24] S. Miyahara and K. Ueda, Thermodynamic properties of the three-dimensional orthogonal dimer model for SrCu$_2$(BO$_3$)$_2$, J. Phys. Soc. Jpn. (Suppl.) B **69**, 72 (2000).

[25] S. Miyahara and K. Ueda, Theory of the orthogonal dimer Heisenberg spin model for SrCu$_2$(BO$_3$)$_2$, J. Phys.: Condens. Matter **15**, R327 (2003).

[26] Zheng Weihong, C. J. Hamer, and J. Oitmaa, Series expansions for a Heisenberg antiferromagnetic model for $SrCu_2(BO_3)_2$, Phys. Rev. B **60**, 6608 (1999).

[27] C. Knetter, A. Bühler, E. Müller-Hartmann, and G. S. Uhrig, Dispersion and Symmetry of Bound States in the Shastry-Sutherland Model, Phys. Rev. Lett. **85**, 3958 (2000).

[28] A. Honecker, S. Wessel, R. Kerkdyk, T. Pruschke, F. Mila, and B. Normand, Thermodynamic properties of highly frustrated quantum spin ladders: Influence of many-particle bound states, Phys. Rev. B **93**, 054408 (2016).

[29] F. Alet, K. Damle, and S. Pujari, Sign-Problem-Free Monte Carlo Simulation of Certain Frustrated Quantum Magnets, Phys. Rev. Lett. **117**, 197203 (2016).

[30] K.-K. Ng and M.-F. Yang, Field-induced quantum phases in a frustrated spin-dimer model: A sign-problem-free quantum Monte Carlo study, Phys. Rev. B **95**, 064431 (2017).

[31] S. Wessel, B. Normand, F. Mila, and A. Honecker, Efficient quantum Monte Carlo simulations of highly frustrated magnets: the frustrated spin-1/2 ladder, SciPost Phys. **3**, 005 (2017).

[32] J. Stapmanns, P. Corboz, F. Mila, A. Honecker, B. Normand, and S. Wessel, Thermal Critical Points and Quantum Critical End Point in the Frustrated Bilayer Heisenberg Antiferromagnet, Phys. Rev. Lett. **121**, 127201 (2018).

[33] H.-Q. Lin and J. L. Shen, Exact ground states and excited states of net spin models, J. Phys. Soc. Jpn. **69**, 878 (2000).

[34] H. Q. Lin, J. L. Shen, and H. Y. Shik, Exactly soluble quantum spin models on a double layer: The net spin model, Phys. Rev. B **66**, 184402 (2002).

[35] J. Richter, O. Derzhko, and T. Krokhmalskii, Finite-temperature order-disorder phase transition in a frustrated bilayer quantum Heisenberg antiferromagnet in strong magnetic fields, Phys. Rev. B **74**, 144430 (2006).

[36] O. Derzhko, J. Richter, A. Honecker, and H.-J. Schmidt, Universal properties of highly frustrated quantum magnets in strong magnetic fields, Low Temp. Phys. **33**, 745 (2007).

[37] O. Derzhko, T. Krokhmalskii, and J. Richter, Emergent Ising degrees of freedom in frustrated two-leg ladder and bilayer $s = 1/2$ Heisenberg antiferromagnets, Phys. Rev. B **82**, 214412 (2010).

[38] E. Müller-Hartmann, R. R. P. Singh, C. Knetter, and G. S. Uhrig, Exact Demonstration of Magnetization Plateaus and First-Order Dimer-Néel Phase Transitions in a Modified Shastry-Sutherland Model for $SrCu_2(BO_3)_2$, Phys. Rev. Lett. **84**, 1808 (2000).

[39] P. Corboz and F. Mila, Tensor network study of the Shastry-Sutherland model in zero magnetic field, Phys. Rev. B **87**, 115144 (2013).

[40] A. Koga and N. Kawakami, Quantum Phase Transitions in the Shastry-Sutherland Model for $SrCu_2(BO_3)_2$, Phys. Rev. Lett. **84**, 4461 (2000).

[41] Y. Takushima, A. Koga, and N. Kawakami, Competing spin-gap phases in a frustrated quantum spin system in two dimensions, J. Phys. Soc. Jpn. **70**, 1369 (2001).

[42] A. Läuchli, S. Wessel, and M. Sigrist, Phase diagram of the quadrumerized Shastry-Sutherland model, Phys. Rev. B **66**, 014401 (2002).

[43] A. W. Sandvik, Stochastic series expansion method with operator-loop update, Phys. Rev. B **59**, R14157 (1999).

[44] O. F. Syljuåsen and A. W. Sandvik, Quantum Monte Carlo with directed loops, Phys. Rev. E **66**, 046701 (2002).

[45] F. Alet, S. Wessel, and M. Troyer, Generalized directed loop method for quantum Monte Carlo simulations, Phys. Rev. E **71**, 036706 (2005).

[46] H. G. Evertz, The loop algorithm, Adv. Phys. **52**, 1 (2003).

[47] M. Troyer and U.-J. Wiese, Computational Complexity and Fundamental Limitations to Fermionic Quantum Monte Carlo Simulations, Phys. Rev. Lett. **94**, 170201 (2005).

[48] B. Bleaney, F. R. S., and K. D. Bowers, Anomalous paramagnetism of copper acetate, Proc. R. Soc. London, Ser. A **214**, 451 (1952).

[49] D. C. Johnston, R. K. Kremer, M. Troyer, X. Wang, A. Klümper, S. L. Bud'ko, A. F. Panchula, and P. C. Canfield, Thermodynamics of spin $S = 1/2$ antiferromagnetic uniform and alternating-exchange Heisenberg chains, Phys. Rev. B **61**, 9558 (2000).

[50] J. Deisenhofer, R. M. Eremina, A. Pimenov, T. Gavrilova, H. Berger, M. Johnsson, P. Lemmens, H.-A. Krug von Nidda, A. Loidl, K.-S. Lee, and M.-H. Whangbo, Structural and magnetic dimers in the spin-gapped system $CuTe_2O_5$, Phys. Rev. B **74**, 174421 (2006).

[51] B. Bernu and G. Misguich, Specific heat and high-temperature series of lattice models: Interpolation scheme and examples on quantum spin systems in one and two dimensions, Phys. Rev. B **63**, 134409 (2001).

[52] B. Bernu and C. Lhuillier, Spin Susceptibility of Quantum Magnets from High to Low Temperatures, Phys. Rev. Lett. **114**, 057201 (2015).

[53] H.-J. Schmidt, A. Hauser, A. Lohmann, and J. Richter, Interpolation between low and high temperatures of the specific heat for spin systems, Phys. Rev. E **95**, 042110 (2017).

[54] Y. Fukumoto, Two-triplet-dimer excitation spectra in the Shastry-Sutherland model for $SrCu_2(BO_3)_2$, J. Phys. Soc. Jpn. **69**, 2755 (2000).

[55] K. Totsuka, S. Miyahara, and K. Ueda, Low-Lying Magnetic Excitation of the Shastry-Sutherland Model, Phys. Rev. Lett. **86**, 520 (2001).

[56] J. Schnack, J. Schulenburg, and J. Richter, Magnetism of the $N = 42$ kagome lattice antiferromagnet, Phys. Rev. B **98**, 094423 (2018).

[57] F. Verstraete and J. I. Cirac, Renormalization algorithms for quantum-many body systems in two and higher dimensions, arXiv:cond-mat/0407066.

[58] Y. Nishio, N. Maeshima, A. Gendiar, and T. Nishino, Tensor product variational formulation for quantum systems, arXiv:cond-mat/0401115.

[59] J. Jordan, R. Orús, G. Vidal, F. Verstraete, and J. I. Cirac, Classical Simulation of Infinite-Size Quantum Lattice Systems in Two Spatial Dimensions, Phys. Rev. Lett. **101**, 250602 (2008).

[60] P. Corboz, T. M. Rice, and M. Troyer, Competing states in the t-J Model: Uniform d-Wave State versus Stripe State, Phys. Rev. Lett. **113**, 046402 (2014).

[61] T. Nishino and K. Okunishi, Corner transfer matrix renormalization group method, J. Phys. Soc. Jpn. **65**, 891 (1996).

[62] R. Orús and G. Vidal, Simulation of two-dimensional quantum systems on an infinite lattice revisited: Corner transfer matrix for tensor contraction, Phys. Rev. B **80**, 094403 (2009).

[63] S. Singh, R. N. C. Pfeifer, and G. Vidal, Tensor network states and algorithms in the presence of a global U(1) symmetry, Phys. Rev. B **83**, 115125 (2011).

[64] B. Bauer, P. Corboz, R. Orús, and M. Troyer, Implementing global Abelian symmetries in projected entangled-pair state algorithms, Phys. Rev. B **83**, 125106 (2011).

[65] P. Corboz, Variational optimization with infinite projected entangled-pair states, Phys. Rev. B **94**, 035133 (2016).

[66] H. C. Jiang, Z. Y. Weng, and T. Xiang, Accurate Determination of Tensor Network State of Quantum Lattice Models in Two Dimensions, Phys. Rev. Lett. **101**, 090603 (2008).

[67] P. Corboz, R. Orús, B. Bauer, and G. Vidal, Simulation of strongly correlated fermions in two spatial dimensions with fermionic projected entangled-pair states, Phys. Rev. B **81**, 165104 (2010).

[68] H. N. Phien, J. A. Bengua, H. D. Tuan, P. Corboz, and R. Orús, Infinite projected entangled pair states algorithm improved: Fast full update and gauge fixing, Phys. Rev. B **92**, 035142 (2015).

[69] P. Corboz, Improved energy extrapolation with infinite projected entangled-pair states applied to the two-dimensional Hubbard model, Phys. Rev. B **93**, 045116 (2016).

[70] A. Lohmann, H.-J. Schmidt, and J. Richter, Tenth-order high-temperature expansion for the susceptibility and the specific heat of spin-*s* Heisenberg models with arbitrary exchange patterns: Application to pyrochlore and kagome magnets, Phys. Rev. B **89**, 014415 (2014).

[71] A. J. Guttmann, Asymptotic analysis of power-series expansions, in *Phase Transitions and Critical Phenomena*, edited by C. Domb and J. L. Lebowitz (Academic Press, London, 1989), Vol. 13.